ELSEVIER

Soil Dynamics and Earthquake Engineering 23 (2003) 349–365

SOIL DYNAMICS AND EARTHQUAKE ENGINEERING

www.elsevier.com/locate/soildyn

Decoupled seismic analysis of an earth dam

Ernesto Cascone*, Sebastiano Rampello

Dipartimento di Costruzioni e Tecnologie Avanzate, Facoltà di Ingegneria, University of Messina, Salita Sperone, 31, S. Agata, Messina 98166, Italy

Accepted 5 February 2003

Abstract

The seismic stability of an earth dam is evaluated via the decoupled displacement analysis using the accelerograms obtained by ground response analysis to compute the earthquake-induced displacements. The response analysis of the dam is carried out under both 1D and 2D conditions, incorporating the non-linear soil behaviour through the equivalent linear method. Ten artificial and five real accelerograms were used as input motions and four different depths were assumed for the bedrock.

1D and 2D response analyses were in a fair agreement with the exception of the top third of the dam where only a 2D modelling of the problem could ensure that the acceleration field is properly described. The acceleration amplification ratio obtained in the 2D analyses was equal to about 2 in all the cases considered, consistently with data from real case histories.

The maximum permanent displacements computed by the sliding block analysis were small, being less than 10% of the service freeboard; a satisfactory performance of the dam can then be envisaged for any of the seismic scenarios considered in the analyses.
© 2003 Elsevier Science Ltd. All rights reserved.

Keywords: Earth dam; Displacement analysis; Ground response analysis; Earthquake; Seismic slope stability; Equivalent linear method

1. Introduction

The performance of earth structures subjected to seismic action can be evaluated through force-based pseudo-static methods, displacement-based sliding block methods, possibly including non-linear soil behaviour, and fully coupled effective stress numerical analyses under dynamic loading. In principle, numerical methods allow the most comprehensive analyses of the response of earth structures to seismic loading. However, reliable numerical analyses require accurate evaluation of soil profile, initial stress state and stress history, pore water pressure conditions, strength and deformation characteristics of the selected soil layers. Moreover, cyclic soil behaviour can be properly described only using advanced constitutive models developed within the framework of bounding surface plasticity or kinematic hardening plasticity, and requiring input parameters not usually measured in field or laboratory testing.

The displacement-based approach provides a compromise between the rather inadequate pseudo-static approach and the more refined numerical analyses; it has indeed the advantage of giving a quantitative assessment of the earthquake-induced displacement using a rather simple analytical procedure.

The displacement analysis can be carried out using the decoupled approach that generally provides a conservative estimate of the seismic-induced permanent displacements [1–4]. In this approach, the deformable response of the earth structure is first accounted for through a dynamic response analysis, and the resulting acceleration time history is then used in a rigid sliding block analysis. The ground response analyses can be performed under 1D or 2D conditions, and the non-linear soil behaviour is usually described through the equivalent linear method that provides a reasonable estimate of soil response for moderate levels of shearing intensity and provided that no significant excess pore water pressure develop during seismic shaking.

The displacement-based approach has been applied in a number of analyses of ideal or real earth dams, rockfill dams and concrete dams [5–9] and, in a few documented case histories, it has been successfully used to back-calculate the measured seismic-induced permanent displacements [10–12].

It is worth noting that the displacement analysis is not capable of reproducing the deformation pattern of an earth structure since actual deformations may be spread out over a zone, leading to bulging rather than sliding. Therefore,

* Corresponding author. Tel.: +39-90-395322; fax: +39-90-395022.
E-mail address: cascone@ingegneria.unime.it (E. Cascone).

0267-7261/03/$ - see front matter © 2003 Elsevier Science Ltd. All rights reserved.
doi:10.1016/S0267-7261(03)00035-6

the computed permanent displacement should be always considered as an index of seismic performance. However, the decoupled approach can provide a useful means for preliminary assessment of the seismic stability of existing dams when significant uncertainties in ground motion and/or material properties require a parametric study to identify the influence of each design assumption and the most critical scenarios.

In this work, the seismic stability of an earth dam has been studied by decoupling the dynamic response analysis from the sliding block analysis. The seismic performance of the dam was first the object of research commissioned to the University of Rome *La Sapienza* [13]. The study was needed since the dam site was classified as non-seismic at construction time, in the late sixties, but was later regarded as a seismic-prone zone. The updated geotechnical characterisation of the earth dam and the foundation soils and some of the results made available by the research allowed further analyses to be performed to evaluate the influence of some design assumptions on the computed response of the dam.

Both artificial and real accelerograms were used as input motions and four different depths were assumed for the bedrock. The results of the analyses confirm that different patterns of behaviour can be obtained depending on the assumed input motion and bedrock depth, thus indicating that the uncertainty of seismological data requires different design assumptions to be investigated to obtain a significant range of possible dam responses.

1D and 2D ground response analyses were in a fair agreement, with the exception of the top third of the dam where only a 2D modelling of the problem properly described the acceleration field. The ratio between the maximum acceleration evaluated in the 2D response analyses and the base acceleration increases in the top third of the dam, attaining values of about 2 at the crest. The acceleration profiles are in agreement with the range of results found in the literature and the maximum values at the crest compare satisfactorily with measured acceleration amplification ratios. The earthquake-induced permanent displacements were much smaller than the service freeboard of the dam, indicating a satisfactory seismic performance of the dam for the seismic scenarios assumed in the analyses.

2. Site description and geotechnical characterisation

The earth dam is located in Puglia, Southern Italy, about 50 km south of the town of Foggia and dikes the course of the Marana Capacciotti stream; it has a volume of about 3.71 Mm^3 and retains 49 Mm^3 of water with a freeboard of about 2.6 m. Fig. 1 shows a plan view of the dam and its main cross-section; the crest is 837 m long, 7.5 m wide, and about 48 m high above the foundation level. The upstream and downstream slopes gradually flatten from 1/2 to about 1/5 at the banks located approximately at the lower third of the dam height. A rockfill cover protects the upstream slope from erosion possibly produced by changes in the water

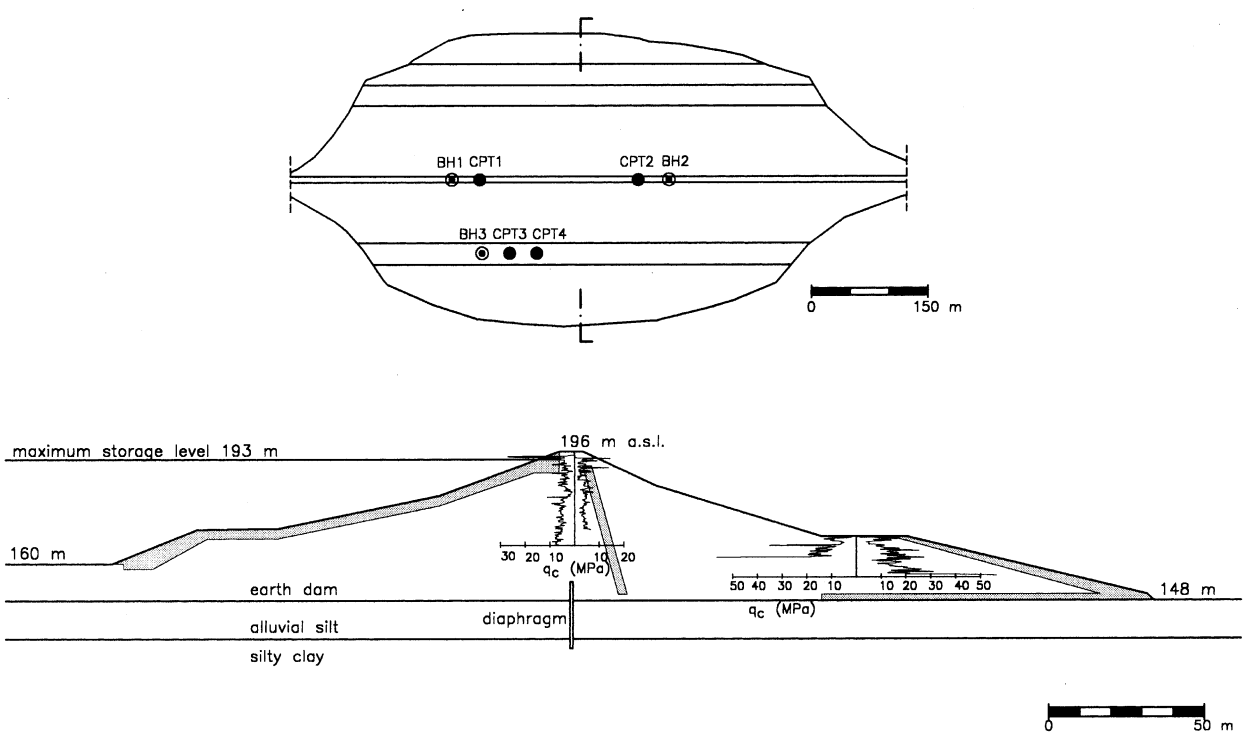

Fig. 1. The Marana Capacciotti dam: plan view and cross-section (adapted from Calabresi et al. [13]).

Table 1
Index and physical properties

	CF (%)	G_s	γ (kN/m^3)	e_0	W_0 (%)	W_L (%)	I_P (%)	I_L
Earth dam	26.3	2.71	20.8	0.515	18.8	36.8	18.7	0.0
Alluvial silt	22.7	2.70	20.4	0.541	20.4	29.8	13.5	0.3
Silty clay	27.5	2.72	20.6	0.553	19.9	33.1	16.0	0.2

level. The drainage system consists of a sub-vertical central drain discharging water into a tunnel parallel to the longitudinal axis of the dam, and of a drain located at the toe of the downstream slope. Seepage through the alluvial soils underlying the dam is prevented by an impervious diaphragm extending into the lower clay deposit.

To study the dam response to earthquake loading a reliable set of stiffness and strength properties was needed and supplementary geotechnical investigations were carried out throughout the earth dam and the foundation soils. Specifically, three boreholes (BH) and four cone penetration tests (CPT) were carried out from the crest and the downstream bank of the dam and laboratory tests were performed on 21 undisturbed tube samples. The soil profile and the geotechnical characterisation of the site are comprehensively reported by Calabresi et al. [13]. The main experimental results are summarised here.

The foundation soil is formed by two layers: an alluvial soil deposit, about 12 m thick, made of medium-stiff silt and clay ($I_L = 0.3$), with thin levels of sand and gravel; a stiff silty clay deposit ($I_L = 0.1$) extending down to the deep bedrock formation. The soil of the earth dam is mainly formed by sandy silt and clay of low plasticity. Table 1 reports the average index properties of the tested soils that are low plasticity, medium to stiff clayey silts.

Table 2 lists the shear strength parameters, cohesion c' and angle of shear resistance φ', as obtained from standard undrained triaxial compression tests and drained direct shear tests, and the values of the undrained shear strength C_u, as obtained from standard unconsolidated undrained triaxial compression tests. Evaluation of the stability conditions via the pseudo-static approach was carried out using conservative values of $c' = 0$ and $\varphi' = 27°$ in the drained analyses and a conservative constant value of $C_u = 166$ kPa in the undrained analyses.

The small-strain shear stiffness was measured in the laboratory by resonant column (RC) tests and bender element (BE) tests carried out under undrained conditions. The RC apparatus was instrumented with a miniaturised

Table 2
Shear strength characteristics

	c' (kPa)	φ' (°)	C_u (kPa)
Earth dam	21–27	27–30	195–312
Alluvial silt	7–25	32	151
Silty clay	60	23	223–230

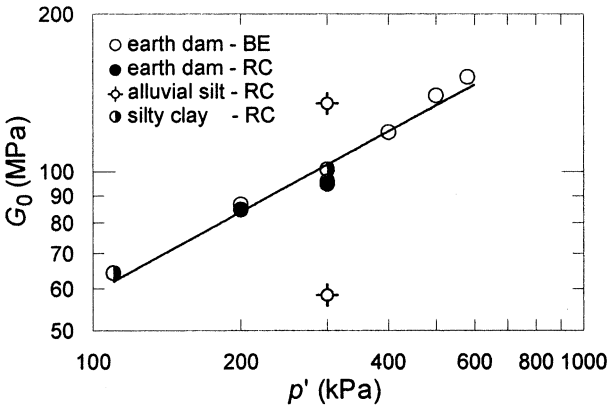

Fig. 2. Small-strain shear stiffness from RC and BE tests (adapted from Calabresi et al. [13]).

pore water pressure transducer installed at the pedestal of the cell. The BEs were installed into the pedestal and the top cap of a stress-path controlled triaxial cell. Samples were confined under isotropic stress conditions at the estimated in situ mean effective stress before testing.

In Fig. 2 the values of the small-strain shear modulus G_0 determined by the RC and the BE tests are plotted in a bilogarithmic scale against the mean effective stress p'. A good agreement is observed between the RC and the BE test results for the samples retrieved from the earth dam. Moreover, values of G_0 for the silty clay deposit plot closely around the best fit line through the BE experimental data of the earth dam. The two RC tests performed on samples from the alluvial silt yield quite different values of G_0 (60 and 135 MPa) consistently with the heterogeneity of the deposit.

Fig. 3 shows the dependency of soil stiffness and damping on strain level as observed in the RC tests.

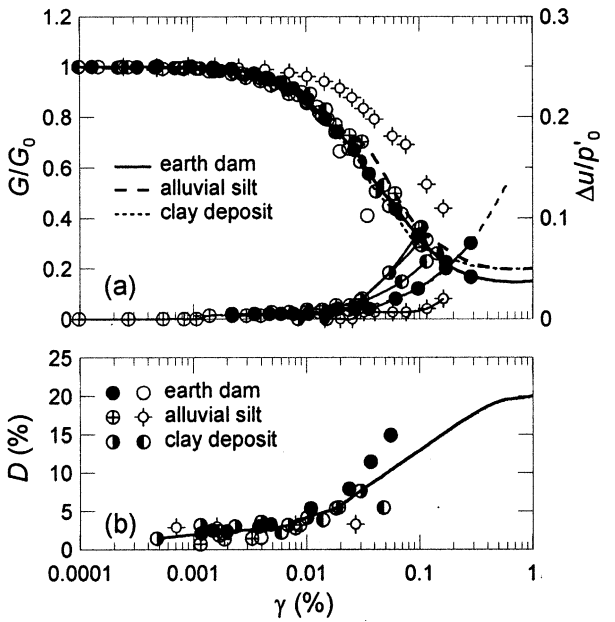

Fig. 3. Non-dimensional shear modulus (a) and damping ratio (b) against shear strain from RC tests (adapted from Calabresi et al. [13]).

The non-dimensional shear modulus G/G_0 is plotted in Fig. 3(a) together with the modulus decay curves assumed for each soil in the ground response analyses. The ratio of the excess pore water pressure to the mean effective stress $\Delta u/p'$ is also shown in the figure. The threshold shear strain γ_ℓ which conventionally bounds the range of linear soil behaviour was taken as the strain corresponding to $G/G_0 = 0.95$; data in Fig. 3(a) show values of $\gamma_\ell = 0.005–0.008\%$. The volumetric threshold shear strain γ_v was assumed to correspond to a ratio $\Delta u/p' = 0.05$; values of γ_v were about 0.2% for the earth dam soil and about 0.1% for the foundation soils. Fig. 3(b) shows the damping ratio D versus the shear strain; experimental data define a narrow band so that a single damping curve was assumed in the ground response analyses.

The profile of the small-strain shear modulus was evaluated using the relationship proposed by Viggiani [14]

$$\frac{G_0}{p_r} = S\left(\frac{p'}{p_r}\right)^n R^m \tag{1}$$

where p' is the mean effective stress, $p_r = 1$ kPa a reference stress, R the overconsolidation ratio, and S, n and m are non-dimensional material constants. In Eq. (1) R is defined as the ratio p'_y/p' where p'_y is the mean effective yield stress determined at the intersection of the unloading–reloading curve through the current state of the soil and the virgin isotropic compression line. The numerical value of the stiffness multiplier S in Eq. (1) depends on the reference stress.

The stiffness exponents were estimated using the empirical relationships relating n and m to the plasticity index I_p [15,16]. The values of the stiffness multiplier S were computed by introducing in Eq. (1) the experimental values of G_0. The stiffness coefficients adopted in the analyses are reported in Table 3 together with the values of the overconsolidation ratios assumed for each layer. Values of R were obtained from the overconsolidation ratio $\mathrm{OCR} = \sigma'_{vmax}/\sigma'_v$ using the relationships

$$R = \mathrm{OCR}\frac{1 + 2K_0^{nc}}{1 + 2K_0^{oc}} \tag{2}$$

$$K_0^{nc} = 1 - \sin\varphi'$$

$$K_0^{oc} = K_0^{nc}\mathrm{OCR}^{\sin\varphi'}$$

The values of p' to be introduced in Eq. (1) were obtained via a 2D numerical analysis in which the construction stages of the dam and the actual hydraulic conditions were modelled [13].

Table 3
Stiffness coefficients

	OCR	φ' (°)	R	m	n	S
Earth dam	1.0	28	1.0	–	0.75	1573
Alluvial silt	1.0	32	1.0	–	0.73	2155
Silty clay	1.5	23	1.3	0.19	0.73	2000

3. Choice of input motion

Assessment of the seismic stability of earth dams requires preliminary specification of input ground motion that generally involves seismic hazard analysis and ground response analysis. The latter may yield reliable results if an accurate geotechnical characterisation of the site is available.

For evaluating the seismic stability of the Marana Capacciotti earth dam, both artificial and real accelerograms were considered in the analyses.

Artificial accelerograms are often used in seismic analysis of earth dams [12,17,18]. In this work, the accelerograms were artificially generated to match the response spectrum provided by the Eurocode No. 8 (EC8) for soil-type A, that is for rock or rock-like formations whose average shear wave velocity in the first 30 m is larger than 800 m/s [19].

Starting from the elastic response spectrum, first the power spectral density (PSD) function, which for soil type A is characterised by a predominant period $T_P = 0.4$ s, was evaluated using the approximate method proposed by Cacciola et al. [20]. Then the artificial accelerograms consistent with the elastic response spectrum were generated using the procedure proposed by Shinozuka [21] in which the accelerograms are obtained by superposition of $N > 400$ harmonic functions having different random phases.

Following the procedures mentioned previously, a set of 10 artificial accelerograms was obtained once the peak ground acceleration and the duration of the event were specified. A peak ground acceleration $a_{max} = 0.35g$ was assumed in the analysis using the results of a seismic hazard study carried out by the Italian National Research Council [22] which, for a return period of 475 years, predicts at the site peak ground accelerations of $0.28–0.32g$. The duration selected for the acceleration time histories was of 30 s: 5 s of initial build-up, 20 s of stationary strong motion and 5 s of final decay.

The main characteristics of the artificial accelerograms used in the analysis are summarised in Table 4. For each accelerogram, the peak ground acceleration and

Table 4
Characteristics of artificial accelerograms

No.	a_{max} (g)	v_{max} (m/s)	I_A (m/s)	T_P (s)	T_D (s)
1	0.31	0.30	4.00	0.43	26.8
2	0.38	0.33	3.97	0.48	27.7
3	0.37	0.32	3.52	0.30	27.3
4	0.33	0.34	3.96	0.38	27.4
5	0.30	0.31	3.88	0.42	27.7
6	0.37	0.32	3.96	0.43	26.9
7	0.35	0.25	4.06	0.28	27.0
8	0.53	0.40	4.67	0.39	27.0
9	0.38	0.33	4.27	0.39	27.0
10	0.34	0.32	3.96	0.41	27.7

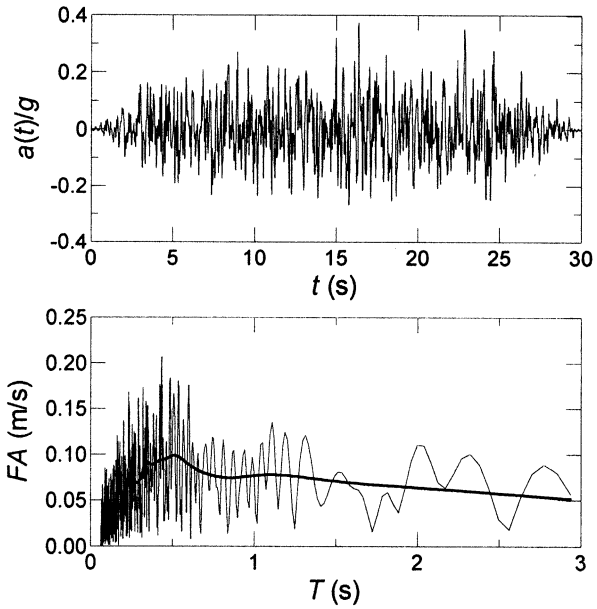

Fig. 4. Accelerogram No.6: acceleration time history and FA spectrum.

the predominant period slightly differ from the reference values of $a_{max} = 0.35g$ and $T_P = 0.4$ s, that, conversely, are approached by the mean values obtained for the whole set of events. The accelerograms are characterised by similar values of the Arias intensity $I_A = 3.5–4.7$ m/s as it could be anticipated since a single PSD function was used in the generation procedure. Accordingly, the artificial accelerograms as well as the Fourier amplitude spectra (FA) show similar trends; an example is given in Fig. 4 for the accelerogram No. 6. The artificial accelerograms are characterised by a significant duration of the strong motion phase and by a wide range of frequencies. In fact the bracketed duration, defined as the time between the first and last exceedances of a threshold acceleration, set equal to $0.05g$, is $T_D \cong 27$ s, and the FA spectrum has the typical shape of a wide-band motion. In Fig. 5, a good agreement is observed between the elastic response spectrum of EC8 for soil type A and the average response spectrum obtained from the 10 acceleration time histories, the consistency prescriptions of Eurocode No. 8 being satisfied. Spectrum

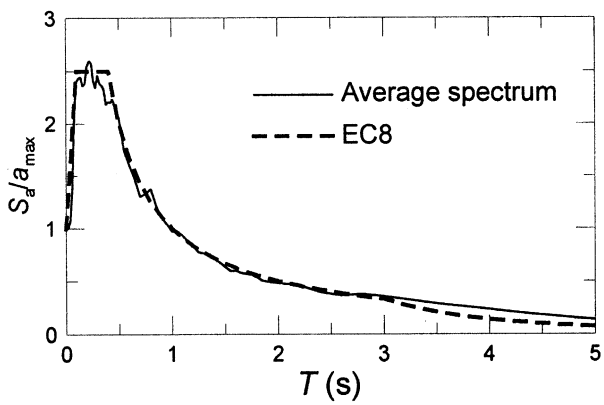

Fig. 5. Comparison of EC8 and computed average elastic response spectra.

Table 5
Characteristics of real earthquake records scaled to $0.35g$

No.	Site	Record	v_{max} (m/s)	I_A (m/s)	T_P (s)	T_D (s)
1	Nocera Umbra '97	Ra01168EW	0.44	1.44	0.38	8.1
2	Tolmezzo '76	AmbiestaEW	0.36	1.42	0.68	6.2
3	Loma Prieta '89	Corral90	0.34	1.38	0.75	14.3
4	Loma Prieta '89	GavTow0	0.26	0.69	0.38	8.6
5	Loma Prieta '89	UCSC90	0.19	1.50	0.16	14.1

compatible time histories adequately represent far-fault ground motions; near-fault motions are in fact generally characterised by high-amplitude long-period pulses of brief duration [23].

Five real ground acceleration records with an energy content matching the response spectra given by Eurocode No. 8 [19] for soil type A, and with values of a_{max} in the range of $0.3–0.5g$ were selected from a database of earthquake records [24,25]. In the ground response analysis, the peak ground acceleration of each real accelerogram was scaled to the same value of $a_{max} = 0.35g$ adopted for the artificial ones. The main characteristics of the selected earthquake records are listed in Table 5, while only the accelerograms recorded at Tolmezzo and at Loma Prieta (Corral90) together with the FA spectra are shown in Fig. 6. The duration of the strong motion phase is of 6–14 s, while the Arias intensity is $I_A = 0.69–1.50$ m/s; these values are significantly lower than those of the artificial accelerograms. The FA spectra of the real earthquake records show a well defined predominant period; moreover, the set of records describe a wide range of the frequency content.

4. Analysis procedure

The displacement-based approach was adopted according to the following procedure:

- the most critical slip surfaces and the corresponding yield accelerations were determined through the pseudo-static approach;
- the initial state of effective stress was first computed via a static 2D numerical analysis to evaluate the small-strain shear modulus G_0 through Eq. (1);
- 1D ground response analyses of the foundation soils were carried out, using the design accelerograms as outcropping input motions; the seismic motion underneath the 12 m thick layer of alluvial silt was then obtained assuming four possible depths of the bedrock;
- 1D and 2D response analyses of the dam and of the alluvial silt layer were carried out using the motions obtained in the previous step;
- displacements of the potential sliding masses were computed using the acceleration time histories evaluated via the 1D and 2D response analyses.

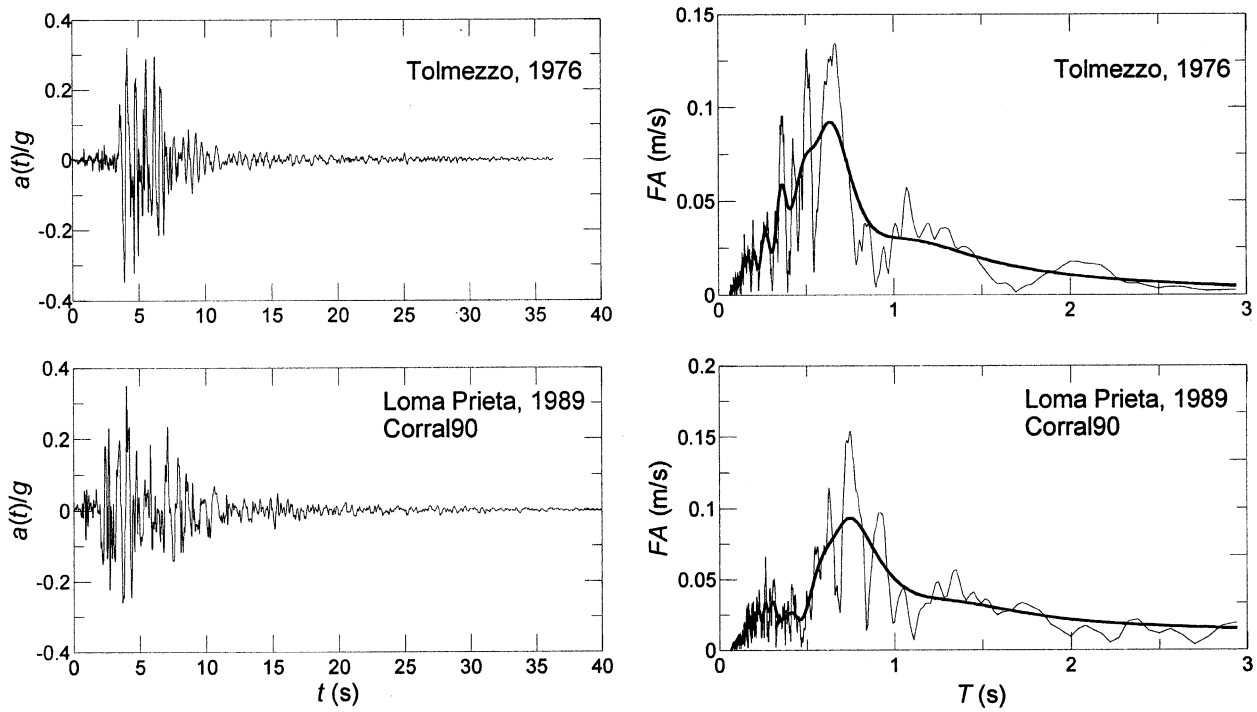

Fig. 6. Selected earthquake records scaled to 0.35g.

The first two steps are part of the studies carried out by Calabresi et al. [13] and are briefly summarised in the following.

The pseudo-static approach was used to evaluate the critical acceleration coefficient k_c and the associated failure surface corresponding to a condition of incipient movement ($F_S = 1$) for the upstream and the downstream slopes. Both total stress undrained analyses and effective stress drained analyses were carried out accounting, in the latter, for the unconfined seepage flow through the dam. Assuming drained conditions implies no excess pore water pressure in the dam that is, consistently, values of the shear strain γ less than the volumetric threshold shear strain γ_v; this occurrence is discussed in the following sections. The critical sliding surfaces are shown in Fig. 7: in the undrained analysis a critical downstream sliding surface was obtained with $k_c = 0.158$, while the drained analysis yielded a value of $k_c = 0.153$ associated with an upstream critical sliding surface [13]. The downstream failure surface is rather deep extending through the layer of alluvial silt, consistently with an undrained shear strength constant with depth, while the upstream failure surface is relatively shallow and entirely comprised in the earth-dam body, as a result of a drained shear strength increasing with depth. Effective stress drained analysis yield the most realistic failure mechanism in that effective stresses are smaller in the upstream portion of the dam.

The initial state of effective stress, needed to evaluate G_0 in the earth dam body and in the foundation soils, was obtained from a static 2D numerical analysis in which the dam construction, the reservoir impoundment and the unconfined seepage through the dam were modelled [13]. Fig. 8(a)–(b) shows the contour lines of pore water pressure and mean effective stress in the dam and in the layer of

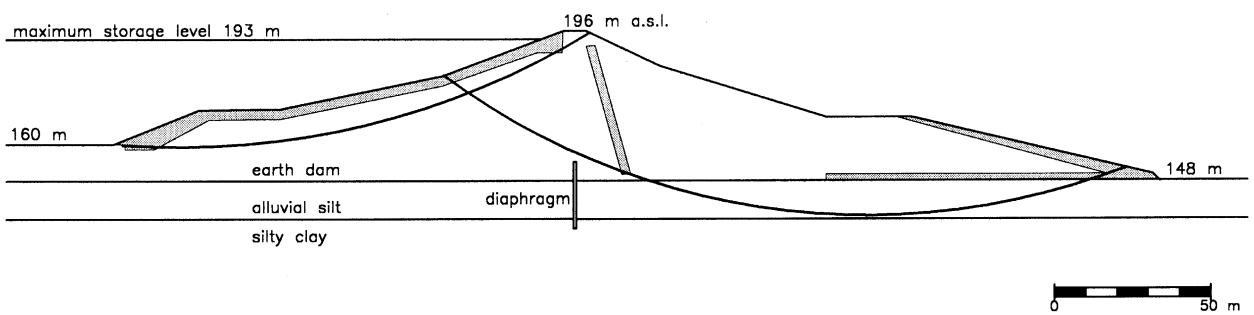

Fig. 7. Critical sliding surfaces.

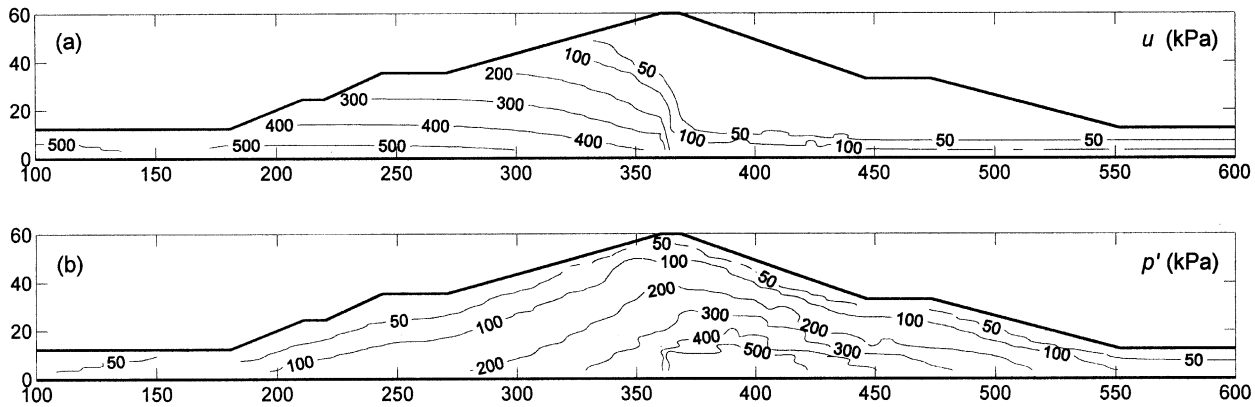

Fig. 8. Contour lines of pore water pressure and mean effective stress.

alluvial silt. The sub-vertical central drain limits the flow domain to the upstream side of the dam. The contours of mean effective stress are bell-shaped showing a maximum value of about 500 kPa at the base of the dam.

5. Ground response analysis of the foundation soil

To perform a ground response analysis, the depth of the bedrock to which the input accelerogram is applied must be specified. For the case at hand, available in situ investigations were not deep enough to provide a reliable indication of the bedrock depth. Several scenarios were then considered varying the bedrock depth from $z_B = 12$ m, which corresponds to the contact between the alluvial soils and the stiff clay deposit, to about 100 m under the base of the dam; four cases were studied, locating the bedrock at 12, 25, 50 and 100 m under the base of the dam.

The 1D response of the soil deposit was studied following the scheme of Fig. 9. The input accelerograms were assumed to be applied to a rock outcropping located at the base of the dam (motion (a) in Fig. 9). Motion (c) at the top of the stiff clay deposit was obtained by deconvolution of the outcropping accelerogram to the assumed bedrock (motion (b)) and subsequent propagation of the bedrock accelerogram through the soil deposit. Ground response was studied using the code SHAKE91 [26] that performs the dynamic analysis in the frequency domain; the non-linear stress-strain soil behaviour and the strain dependent damping are described using the linear equivalent procedure and assuming that the soil behaves as a visco-elastic material.

The small-strain shear modulus of the foundation soil to be used in the 1D analyses was determined starting from

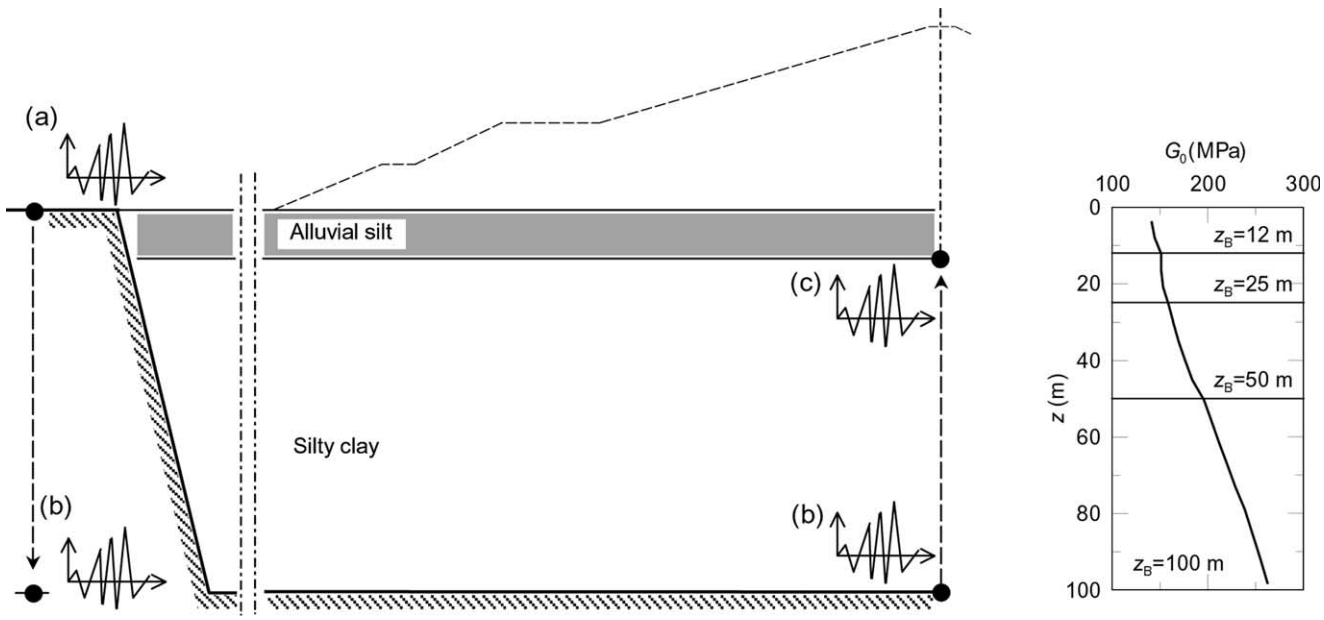

Fig. 9. Scheme of the 1D response analysis of the foundation soil deposit.

the initial state of effective stress provided by the static 2D numerical analysis of the dam construction. Specifically the values of mean effective stress p' were first computed for each element of the mesh and the elemental values of $G_{0(i)}$ were evaluated using Eq. (1). The average shear modulus at small-strains $G_{0(av)}$ was then computed for each depth, i.e. for each row of elements, as the mean of $G_{0(i)}$ weighted on the element width b_i

$$G_{0(av)} = \frac{\sum G_{0(i)} b_i}{\sum b_i} \tag{3}$$

In this way, the confining effect of the dam on the foundation soil was accounted for in the analysis. The profile of $G_{0(av)}$ adopted in the analyses is also shown in Fig. 9.

Figs. 10 and 11 show typical results obtained from the first step of the analysis using the artificial accelerogram No. 6 as input motion. In Fig. 10 the profiles of the non-dimensional acceleration a_{max}/g are plotted for the four assumed bedrock depths z_B. Moving the bedrock upwards, soil column becomes stiffer and de-amplification reduces, a net amplification being observed for $z_B = 12$ m. For any thickness of the soil deposit, increasing values of acceleration are observed in the upper 12–15 m. The amplification functions (AF) computed between the output motion on top of the soil deposit and the one at the outcropping rock are plotted in Fig. 11 against the frequency. Increasing the depth of the bedrock from $z_B = 12$ m to 100 m the deformability of the soil column increases and, consistently, the AF peaks shift towards lower frequencies, the curves shrink and the attenuation phenomena become more pronounced. The maximum values of the AFs are about 2.3 irrespective of the depth of the bedrock as a result of the counter-balancing effects of non-linear behaviour and stiffness inhomogeneity.

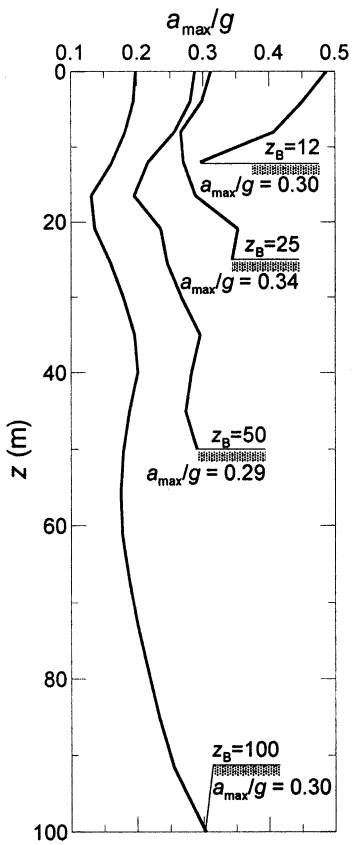

Fig. 10. 1D response analysis of the foundation soil: profiles of a_{max}/g obtained using accelerogram No. 6.

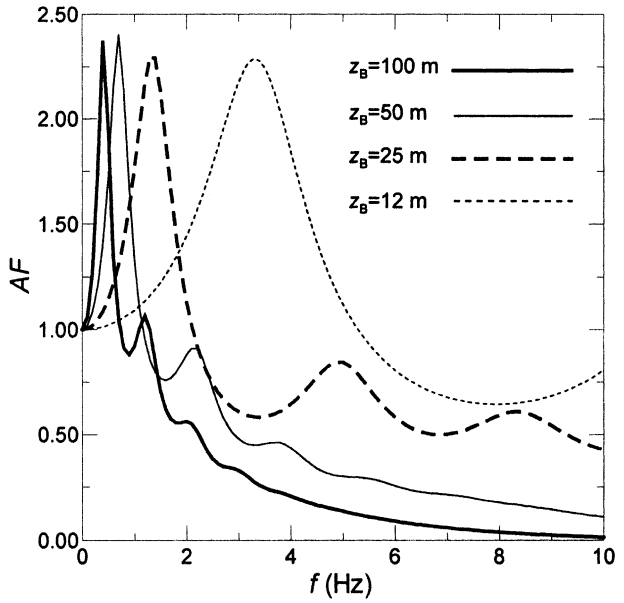

Fig. 11. 1D response analysis of the foundation soil: AFs obtained using accelerogram No. 6.

The main characteristics of the accelerograms obtained at the contact of the alluvial silt with the stiff clay deposit ($z = 12$ m) using the artificial input motion No. 6 are summarised in Table 6. The peak acceleration and the Arias intensity decrease with increasing depths of the bedrock, while the peak velocity and values of T_P increase with z_B. In fact, the accelerogram characteristics change significantly with increasing heights of soil columns resulting in longer natural periods and greater de-amplification effects.

Fig. 12 shows the results of the analyses performed using the scaled real earthquake records as input motions. For

Table 6
Characteristics of accelerograms at $z = 12$ m for input motion No. 6

z_B (m)	a_{max} (g)	v_{max} (m/s)	I_A (m/s)	T_P (s)	T_D (s)
12	0.30	0.28	2.85	0.43	26.8
25	0.27	0.37	2.53	0.60	26.6
50	0.22	0.36	1.60	1.30	24.7
100	0.16	0.38	1.01	2.31	23.1

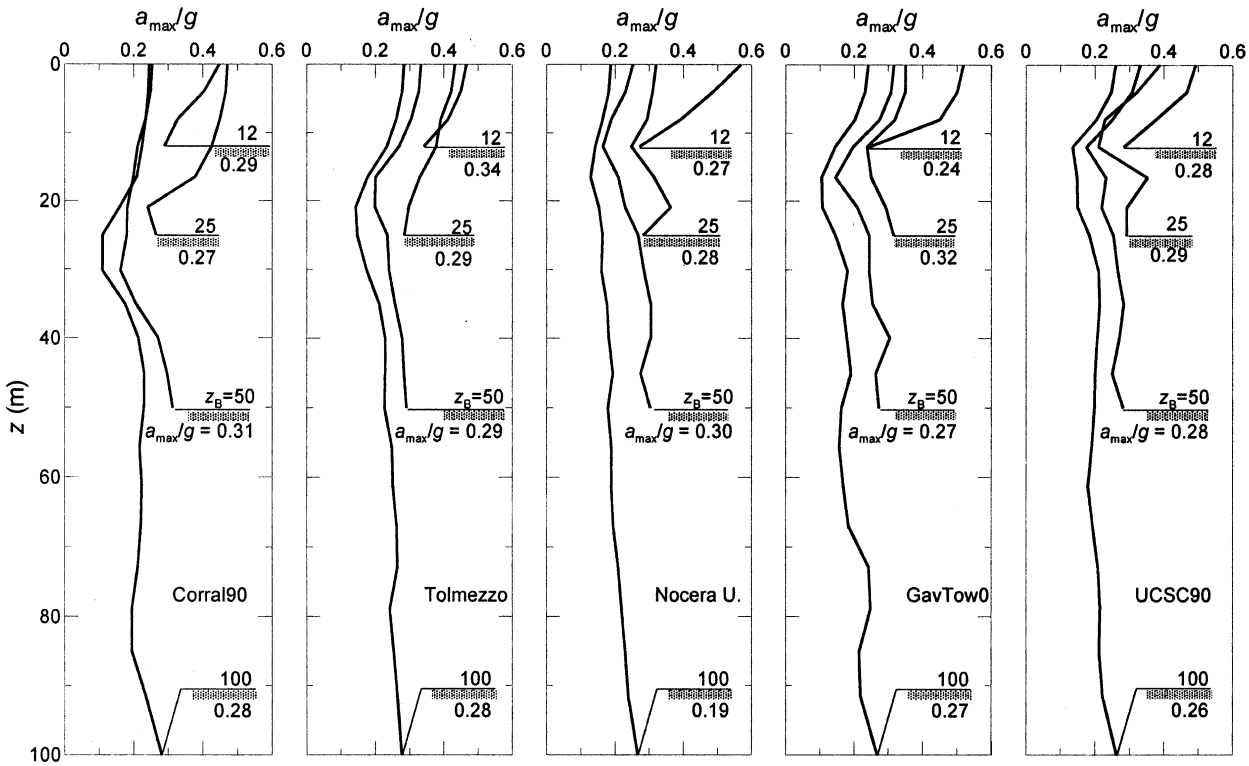

Fig. 12. 1D response analysis of the foundation soil: profiles of a_{max}/g obtained using the scaled real records.

each accelerogram, the acceleration ratio a_{max}/g is plotted against the depth for the four assumed depths of the bedrock. De-amplification effects reduces as soil columns shorten, a net amplification being observed for $z_B = 25$ and 12 m. For $z_B = 12$ m the highest amplification is observed for the records of Nocera Umbra and those named GavTow0 and UCSC90 of Loma Prieta earthquake; this is consistent with values of predominant periods in Table 5 close to the computed natural period of the soil layer, $T = 0.29$ s. For $z_B = 25$ m the highest amplifications are observed for the records of Tolmezzo and the one named Corral90 of Loma Prieta; these events have a predominant period nearly coincident with the natural period of the 25 m-thick soil layer ($T = 0.70$ s). For deeper locations of the bedrock no significant amplification or de-amplification effects are observed.

6. Response analysis of the earth dam

Once the accelerograms at the top of the clay deposit were obtained, the response of the dam was evaluated through both 1D and 2D analyses.

6.1. 1D analysis

In the 1D analysis the dam was modelled as a soil column of the same height of the dam (Fig. 13) and was studied using the code SHAKE91 [26]. The profile of the average small-strain shear modulus $G_{0(av)}$ in the figure was obtained for each horizontal section of the dam following the same averaging procedure described earlier (Eq. (3)); the obtained values were in this case multiplied by the ratio $(4/2.59)^2$ in order to approximate the fundamental period of a horizontal elastic soil deposit ($T_0 = 4H/V_S$) to the fundamental period of the dam, assimilated to an elastic soil wedge ($T_0 = 2.59H/V_S$). Though crude, such an approximation was shown to result in a reasonable agreement with more refined models [27]. The experimental values of the small-strain shear modulus, as obtained from the RC tests carried out on samples retrieved from the dam centre line, are in good agreement with the computed values of G_0. Also in Fig. 13 the ratio of $G_{0(av)}$ to its maximum value at the base $G_{0(B)}$ is plotted against the non-dimensional depth z/H. The computed values of $G_{0(av)}/G_{0(B)}$ are very closely spaced around the curve $G_{0(av)}/G_{0(B)} = (z/H)^{2/3}$ proposed by Gazetas [28] and based on field data obtained from 12 actual earth dams; this result could have been anticipated noting that the exponent n in Eq. (1) is close to 2/3.

The accelerograms used in the sliding block analysis were computed by the response analyses at the depths of the centre of gravity of the two potential sliding masses identified through the pseudo-static analysis. These were $d_{u\text{-}s} = 28$ m and $d_{d\text{-}s} = 33$ m from the crest of the dam for the upstream and the downstream slope, respectively.

For any of the accelerograms used as outcropping input motions, four response analysis were carried out on the foundation soil, one for each of the assumed bedrock depths;

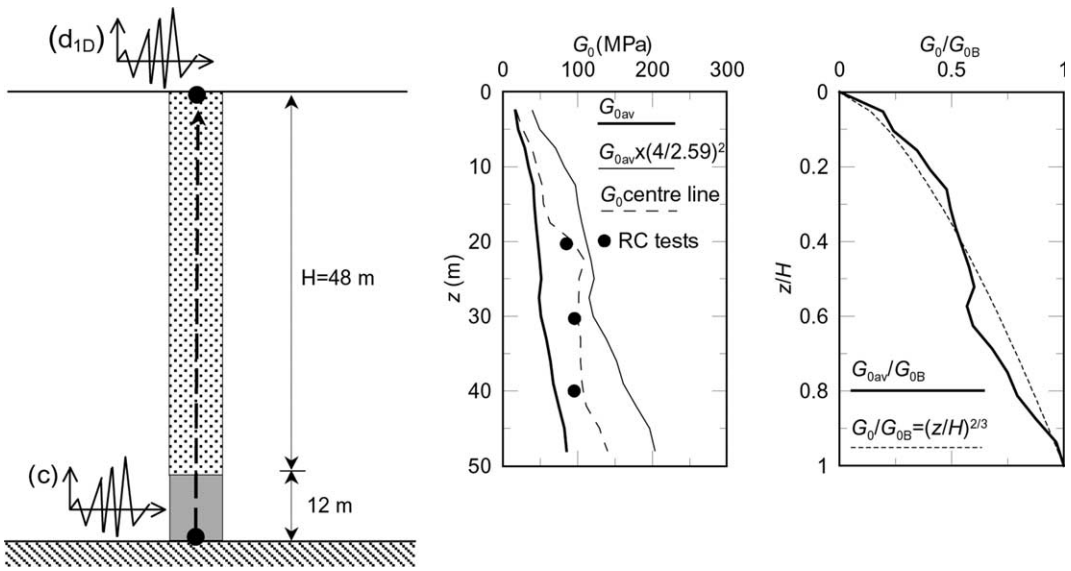

Fig. 13. Scheme of the 1D response analysis of the dam.

accordingly four different accelerograms were obtained at the contact of the alluvial silts with the stiff clay deposit and four response analyses of the dam were performed.

Results of the 1D dynamic response of the dam and of the underlying 12 m thick layer of alluvial silt are presented in Fig. 14 which shows the profiles of a_{max}/g, γ_{av}, τ_{max}, G and D, obtained applying the four acceleration time histories determined at the top of the stiff clay deposit using the artificial accelerogram No. 6 as input motion.

The acceleration profiles exhibit amplification in the upper third of the dam, as typically obtained independently of the input ground motion. The highest values of the ratio a_{crest}/a_{base} are obtained when assuming the bedrock depths at 50 and 100 m, for which the lowest base accelerations are obtained.

The average shear strain in Fig. 14 increases up to values of $\gamma_{av} \leq 0.4\%$ from the crest of the dam down to a depth of about 29 m, where the dam section widens due to the presence of the lateral banks. At greater depths, the shear strain decreases to values of about 0.2% at the dam base. A significant decrease of the shear modulus is observed irrespective of the input motion, the ratio of G/G_0 being about 0.4.

Fig. 15 shows the AFs between the four accelerograms computed at the crest of the dam and those obtained at the top of the stiff clay deposit using the artificial motion No. 6. Amplification is observed for frequencies $f < 2$ Hz, with maximum values of about four attained at $f = 0.6$ Hz, which is the natural frequency of the earth dam as obtained by the linear equivalent method. Unlike the previous analysis (Fig. 11) in this case seismic waves propagate in a soil column of constant height; the differences in the AF curves are less and mainly depend on different characteristics of the input accelerograms (Table 6). The changes

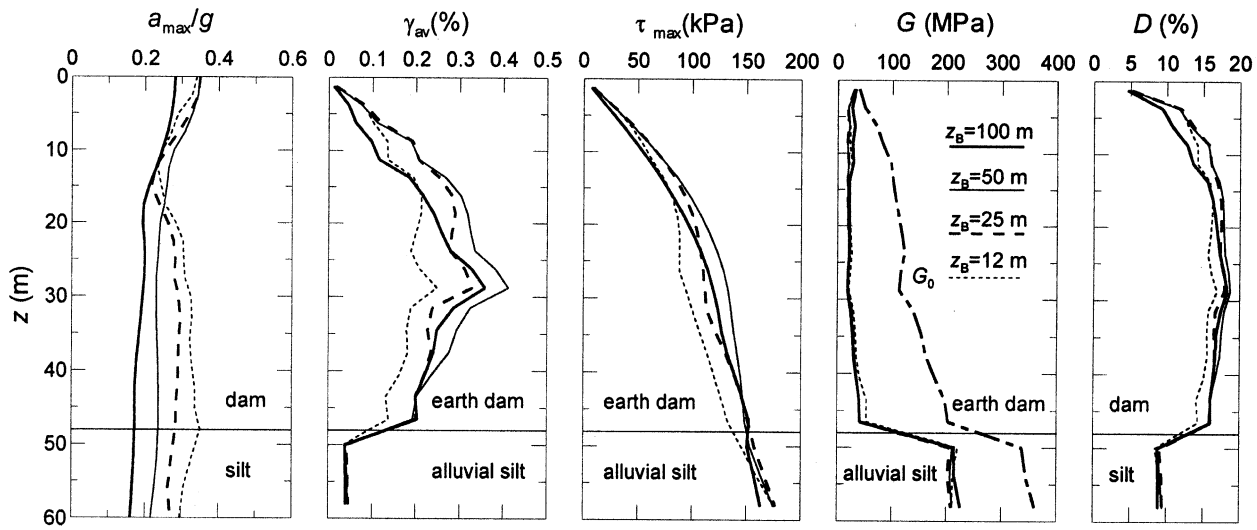

Fig. 14. 1D response analysis of the dam: profiles of a_{max}/g obtained using accelerogram No. 6.

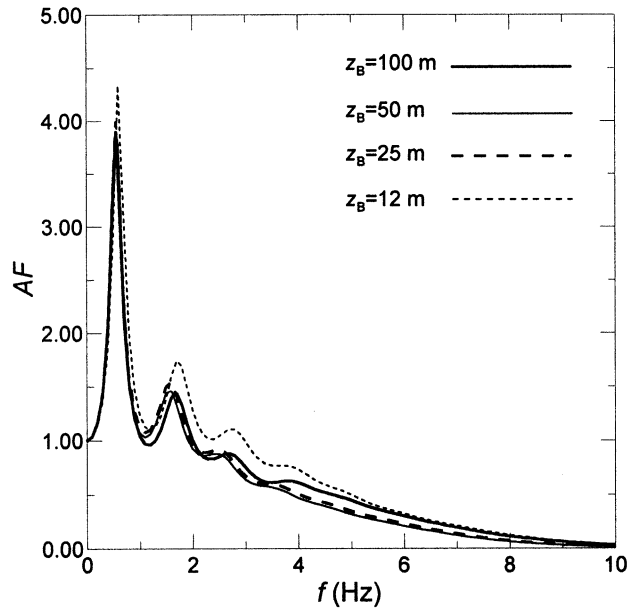

Fig. 15. 1D response analysis of the dam: AFs obtained using accelerogram No. 6.

observed as the bedrock depth was increased from $z_B = 12$ m to $z_B = 100$ m are similar to those discussed for Fig. 11 although less pronounced.

Fig. 16 shows the profiles of non-dimensional maximum acceleration a_{max}/g and average shear strain γ_{av} obtained when accelerograms derived from real earthquake records were used. The maximum acceleration changes slightly from the bottom of the soil column ($z = 60$ m) to a depth of about $z = 30$ m, diminishes substantially attaining minimum values for $z = 15–20$ m and sharply increases in the upper third of the dam; the maximum crest accelerations are in the range $0.28–0.58g$, the maximum values of $0.5–0.6g$ being computed assuming $z_B = 25$ m for the Corral90 and Tolmezzo accelerograms. The average shear strain increases with depth in the upper 10-30 m and then gradually decreases approaching the contact with the alluvial silt. Maximum values of $\gamma_{av} = 0.25–0.4\%$ are obtained assuming the bedrock at a depth of 25 and 50 m. Accelerograms originated from the Corral90, Tolmezzo and Nocera Umbra records gave the highest response in terms of average shear strain. In fact, the Arias intensity and the maximum velocity of these

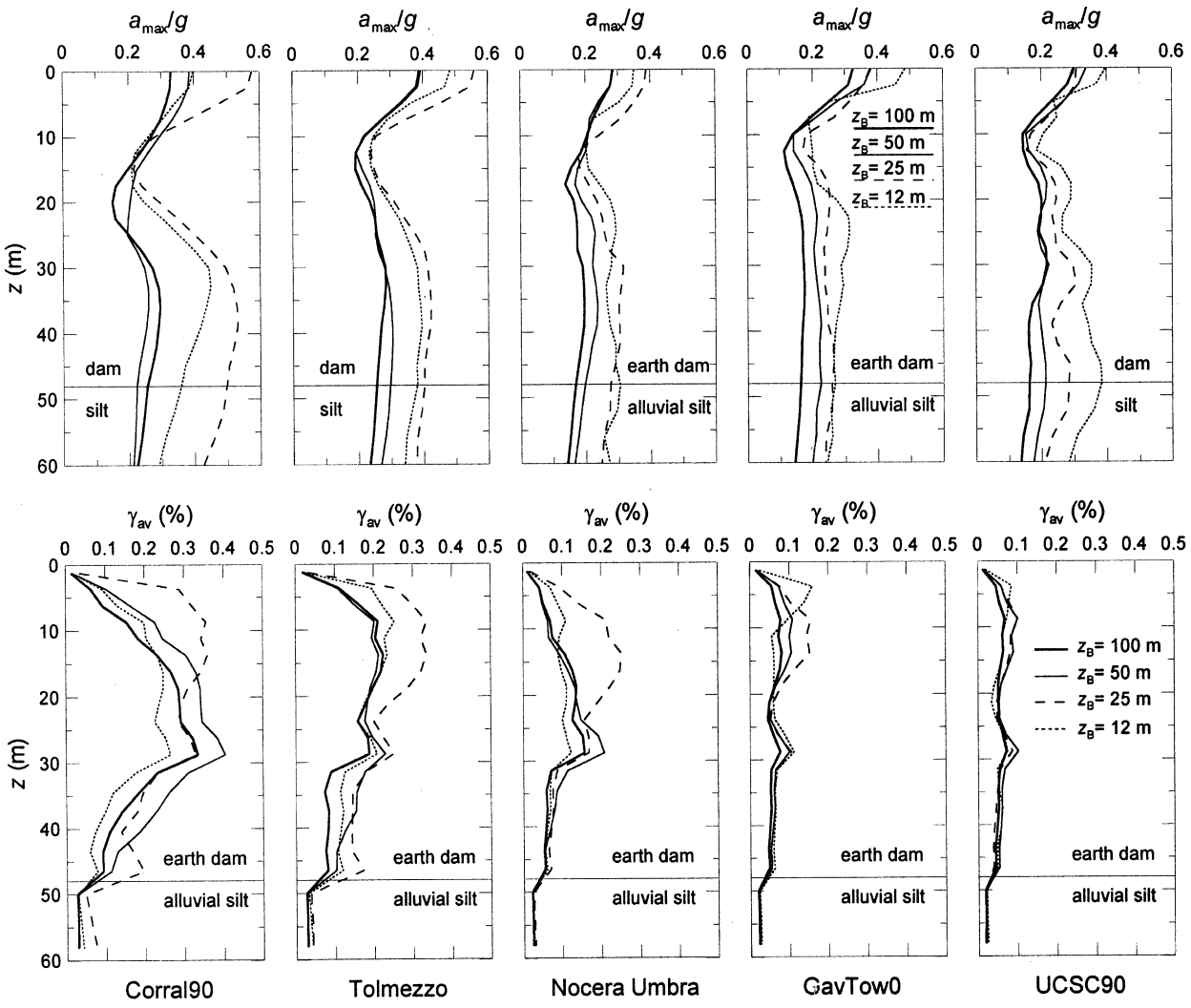

Fig. 16. 1D response analysis of the dam: profiles of a_{max}/g and average shear strain obtained using the scaled real records.

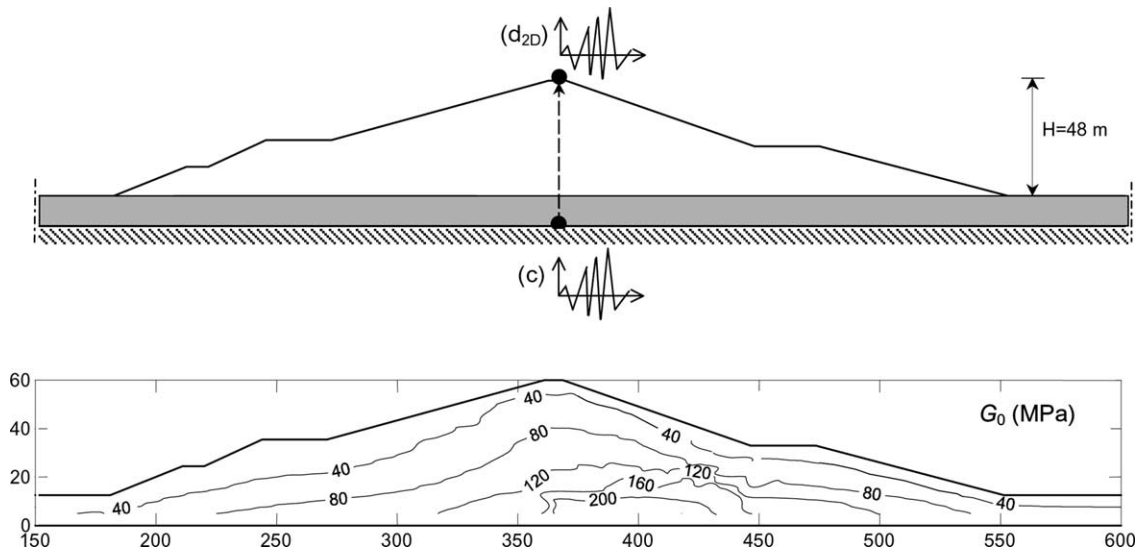

Fig. 17. Scheme of the 2D response analysis of the dam and shear modulus contours.

accelerograms are significantly higher than those relevant to the GavTow0 and UCSC90 records; specifically the ratios between the values of I_A and v_{max} are in the range of 5–7 and of about 2, respectively.

Values of γ_{av} greater than the volumetric threshold $\gamma_v = 0.2\%$ might infer development of excess pore water pressure Δu during seismic shaking. However, measurements of Δu carried out in RC tests indicate that for values of $\gamma \approx 0.4\%$ the excess pore water pressure is small, being about 10% of the mean effective stress (Fig. 3). Moreover, in the downstream portion of the dam the vertical central drain prevent any pore water pressure build-up (Fig. 8), while in the upstream portion excess pore water pressure can only develop underneath the rockfill cover, 3–4 m thick.

6.2. 2D analysis

The 2D response analyses of the dam were carried out using the FE code QUAD4M [29] which performs seismic ground response analysis in the time domain: it includes a compliant base and accounts for non-linear stress–strain soil behaviour and strain dependent damping through the linear equivalent procedure; similarly to SHAKE91, the soil is modelled as a visco-elastic material. The real geometry of the dam and the underlying layer of alluvial silt were considered in the analysis. The FE mesh consisted of 1788 quadrilateral and triangular elements extending 370 m to each side of the dam centre line; a ratio of the mesh to the dam width of about 2 was adopted to minimise boundary effects on soil response. The mesh was fixed at the base, modelled as a transmitting boundary, and was restrained only vertically at the sides to model the free field conditions.

The accelerograms obtained on top of the clay deposit from the 1D ground response analysis of the foundation soils were applied at the base of the mesh as input motions for the 2D response analysis. Elemental values of the shear modulus G_0 were computed through Eq. (1) using the elemental values of p' evaluated in the static 2D numerical analysis. A scheme of the problem is shown in Fig. 17 together with the contour lines of the small-strain shear modulus; consistently with the distribution of p', the contour lines of G_0 are bell-shaped and show values in the range of 40–180 MPa.

The accelerograms resulting from the seismic wave propagation were obtained for several nodes of the mesh. Moreover, the average acceleration time histories to be used in the displacement analysis were determined using the QUAD4M built-in procedure [29]; this, for each time step, evaluates the horizontal and the shear stresses acting on the elements located along the sliding surface, computes the resultant of all the horizontal forces acting on these elements, and divides the resultant horizontal force by the mass of the whole potential sliding body [5].

The 2D response analysis of the earth dam was carried out using five artificial accelerograms (A1–A5) and five real earthquake records (R1–R5). The relevant characteristics of the selected input accelerograms are listed in Table 7 together with the specification of the motion and

Table 7
Characteristics of input accelerograms for the 2D analyses

	Originated from record	z_B (m)	a_{max} (g)	v_{max} (m/s)	I_A (m/s)	T_P (s)	T_D (s)
A1	#9	100	0.17	0.41	0.82	2.73	23.7
A2	#1	25	0.27	0.35	2.67	0.81	25.9
A3	#6	25	0.27	0.37	2.53	0.6	26.6
A4	#4	12	0.31	0.27	2.77	0.58	27.1
A5	#7	25	0.28	0.34	2.69	0.75	25.6
R1	Corral90	25	0.43	0.48	2.37	0.75	11.34
R2	Tolmezzo	25	0.38	0.40	1.72	0.69	7.63
R3	Tolmezzo	50	0.27	0.29	0.75	1.10	5.99
R4	Corral90	50	0.21	0.35	0.89	1.33	9.40
R5	Tolmezzo	12	0.34	0.33	1.19	0.69	6.37

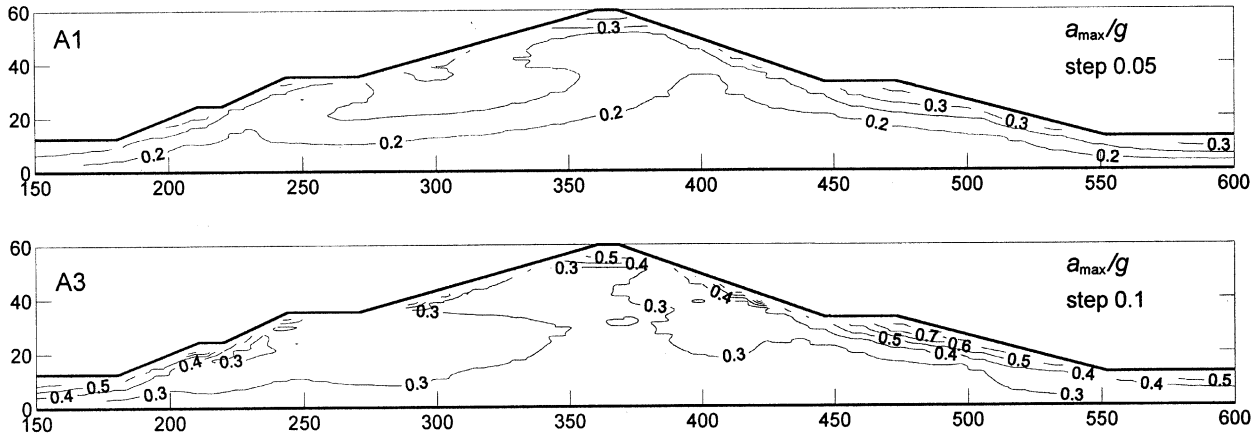

Fig. 18. 2D response analysis of the dam: contour lines of a_{max}/g obtained using the selected artificial accelerograms.

the bedrock depth from which they were originated. Peak acceleration of the input artificial motions A2–A5 are close to $0.3g$ while a value of $a_{max} = 0.17g$ was obtained for motion A1 that exhibits a predominant period $T_P = 2.73$ s, consistent with the filtering effects related to the high thickness assumed for the soil deposit ($z_B = 100$ m). The input real motions R1–R5 have maximum acceleration in the range $0.21–0.43g$ and predominant period in the range $T_P = 0.69–1.33$.

Typical contours of peak acceleration a_{max}/g are plotted at specified step intervals in Figs. 18 and 19 for two artificial (A1 and A3) and two real (R1 and R3) accelerograms. In all cases most of the earth dam is shaken by accelerations lower than $0.2–0.3g$; in fact, values of a_{max}/g as high as 0.6 g are only obtained at a few metres of depth from the side shells due to the low confining stresses, and in the next proximity of the crest due to wave focusing effects.

Consistently with the contours of a_{max}, most of the soil mass in the dam undergoes strain levels lower than 0.3% with the exception of the soil next to the corners of the dam profile, where focusing effects and low confining stresses induce shear strains as high as 0.6% down to a depth of about 8–10 m from the side shells of the dam.

The profiles of peak acceleration and average shear strain obtained along the dam centre line are plotted in Fig. 20 for both the artificial and the real input accelerograms. Peak accelerations do not vary significantly for depths larger than 20 m and exhibit a substantial increase in the upper third of the dam; the maximum values attained at the crest are about twice the input peak acceleration. The average shear strain increases with depth reaching maximum values of $\gamma_{av} \approx 0.5–0.6\%$ for $z = 520$ m and gradually decrease to $\gamma_{av} < 0.15\%$ down to a depth of 60 m.

Again, levels of shear strain higher than the volumetric threshold $\gamma_v = 0.2\%$ might imply pore pressure build-up during the earthquake; a ratio $\Delta u/p' \approx 0.13$ can be evaluated from the RC test results for values of $\gamma \approx 0.6\%$ (Fig. 3). Correspondingly, low values of $\Delta u \leq 7$ kPa can be estimated underneath the upstream slope, at depths of about 10 m (Fig. 8), the associated reductions in effective stress being negligible.

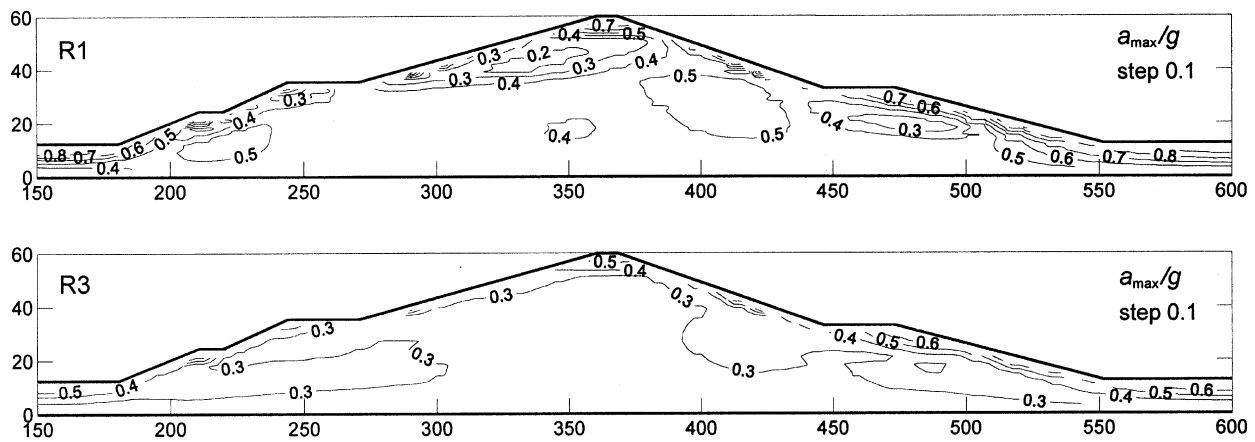

Fig. 19. 2D response analysis of the dam: contour lines of a_{max}/g obtained using the selected real accelerograms.

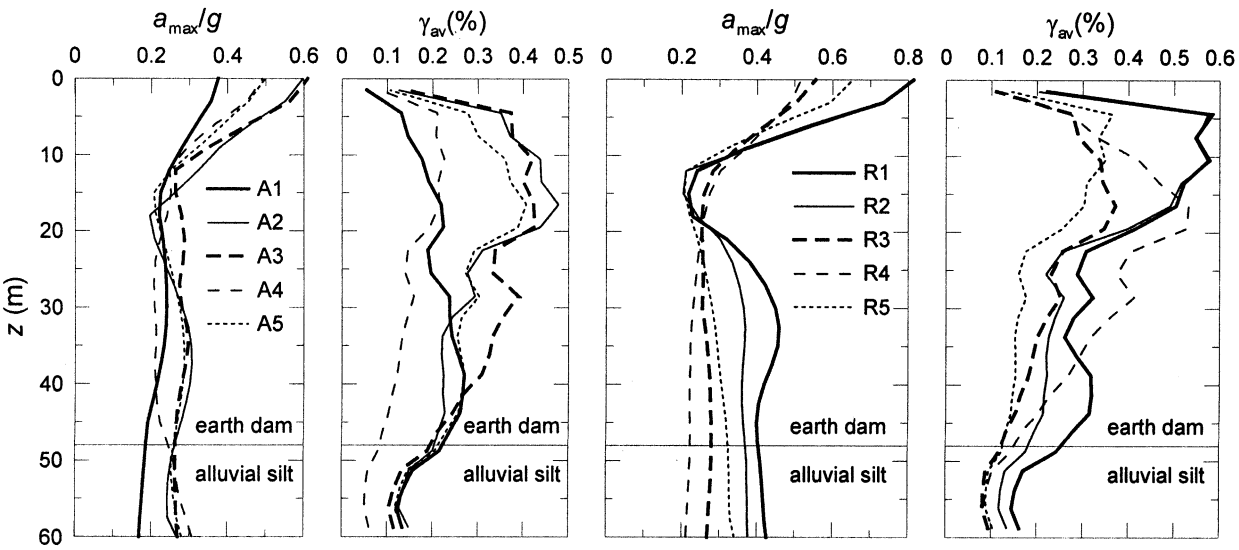

Fig. 20. 2D response analysis of the dam: profiles of a_{max}/g and average shear strain along the dam centre line.

7. Displacement analysis

The seismic stability of the earth dam was expressed in terms of the permanent displacement accumulated during the seismic event, comparing the displacement induced by the input motion with threshold values. The earthquake-induced displacement of the potential sliding mass was evaluated using the sliding block analysis carried out for rotational collapse mechanisms. In the analysis, the potential sliding mass is treated as a rigid plastic body and permanent displacements take place whenever the ground acceleration exceeds the critical value [30]. Despite its extreme simplicity, the method has proved to work satisfactorily provided that the soil behaviour is not strongly non-linear, significant pore water pressures do not develop and the soil resistance is not drastically affected by cyclic degradation [23].

Computed displacements are to be compared with threshold values assumed as tolerable for the dam. Hynes-Griffin and Franklin [31] recommended 100 cm of displacement as a possible upper limit, admitting that such a value should be tolerated in most dams without threatening the integrity of the reservoir, although it could cause serious damage. For the case at hand a maximum displacement of 50 cm was adopted as threshold value, that is about one fifth of the service freeboard of the dam (2.6 m).

The displacements of the potential sliding masses were evaluated using the acceleration time histories obtained by the response analyses for any of the four assumed bedrock depths. More specifically, in the 1D analysis the accelerograms computed at the depth of the centre of gravity of the sliding mass were used in the displacement computations, while in the 2D analysis the average accelerograms through the potential sliding surface were adopted [5]. The displacements were computed using both sides of any accelerogram (normal and reverse shaking) and considering the two critical failure mechanisms obtained from the pseudo-static analyses. In the following, the vertical components of displacement are referred to.

The maximum displacements obtained from the 1D response analyses are summarised in Table 8 that refers to both the artificial and the real motions; in the last row the table also reports the displacements computed using the original accelerograms without carrying out any response analysis. After 1D response analysis, the larger displacements are obtained assuming the bedrock at a depth of 25 m; these are of about 8 and 20 cm for artificial and real input motions, respectively. Neglecting ground response analysis, smaller displacements would have been obtained using the artificial ($d_{max} \approx 5$ cm) and the real accelerograms ($d_{max} \approx 8$ cm). The scaled real acceleration time histories of Tolmezzo and Corral90 yielded the greater displacements.

Table 9 summarises the results of the displacement analysis performed using the average accelerograms computed in the 2D ground response analyses along the potential sliding mass of the upstream slope. The characteristics of these accelerograms are also given in the table for comparison with those of the accelerograms used as input to the 2D analyses. The displacements obtained after

Table 8
Displacement computed from 1D ground response analysis

z_B (m)	Artificial accelerograms		Real accelerograms	
	Upstream d_{max} (cm)	Downstream d_{max} (cm)	Upstream d_{max} (cm)	Downstream d_{max} (cm)
12	3.3	3.8	4.9	8.5
25	5.1	8.1	13.3	20.2
50	4.5	2.4	1.7	2.1
100	8.6	2.1	2.2	3.5
	4.7	5.0	7.6	3.6

Table 9
2D analysis: accelerograms characteristics and displacements of upstream slope

	a_{max} (g)	v_{max} (m/s)	I_A (m/s)	T_P (s)	T_D (s)	$d^{(+)}$ (cm)	$d^{(-)}$ (cm)
$A1_{eq}$	0.20	0.71	2.14	2.00	25.84	0.6	1.6
$A2_{eq}$	0.24	0.50	1.81	1.15	23.49	1.0	3.0
$A3_{eq}$	0.21	0.49	2.36	2.00	25.75	1.4	1.9
$A4_{eq}$	0.16	0.32	1.44	1.43	23.74	0.1	0
$A5_{eq}$	0.21	0.48	2.25	1.76	24.34	1.6	0.5
$R1_{eq}$	0.20	0.19	1.17	0.93	9.46	0.3	1.4
$R2_{eq}$	0.21	0.26	0.56	1.10	5.82	0.2	0.6
$R3_{eq}$	0.21	0.33	0.86	1.33	7.83	0.2	1.0
$R4_{eq}$	0.23	0.24	1.01	1.33	10.26	0.4	2.3
$R5_{eq}$	0.18	0.23	0.44	1.10	5.80	0.1	0

2D response analyses are as much as about five times less than those computed after 1D response analysis. A maximum vertical displacement of about 3 cm is obtained for the upstream slope, while no displacements are computed for the downstream potential sliding mass; these latter result can be attributed to the low acceleration levels induced by seismic shaking along the deep seated sliding surface.

For any of the cases considered earlier, the computed displacements resulted well below the threshold value of 50 cm assumed as tolerable for the earth dam.

8. Discussion and conclusions

The response analysis of the earth dam was carried out under both 1D and 2D conditions; the former assumption is a simple crude idealisation of the problem while the latter assumption is valid for long dams subjected to a synchronous base excitation. For the examined dam the aspect ratio L/H is equal to about 17 and the 3D stiffening effects due to the abutments, which induce an increase in natural frequencies and crest acceleration, can be neglected. The seismic shaking is the result of a number of body and surface waves and the motion generally differs from point to point; however, the effect of motion incoherence appears to be beneficial to the dam response [7].

Fig. 21 shows, for both artificial and real accelerograms, the profiles of the maximum acceleration ratio a_{max2D}/a_{max1D} where a_{max2D} is the acceleration computed at the dam centre line in the 2D response analyses and a_{max1D} the acceleration obtained in the 1D response analyses. It is apparent that in the top third of the dam the acceleration ratio increases up to about 1.3–1.7 at the dam crest. This occurrence, typically obtained in dam response analyses, can be attributed to the increasing influence of both the 2D geometry of the problem and the wave focusing effects as the top of the dam is approached. Consistently, a better agreement between 1D and 2D ground response analyses, with differences

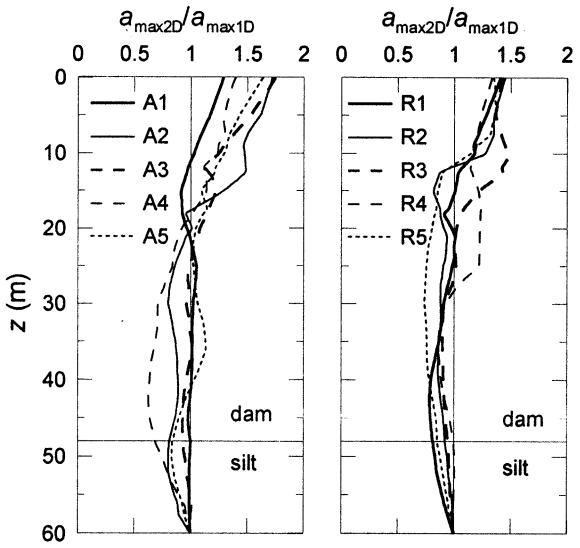

Fig. 21. Comparison between 2D and 1D profiles of a_{max}/g.

generally lower than about 20%, is observed as the dam width increases ($z \geq 20$ m).

Fig. 22 shows the profiles of the acceleration amplification ratio a_{max}/a_{base}, where a_{max} and a_{base} are the maximum accelerations along the dam centre line and at the dam base, both obtained from 2D response analyses. Artificial and real accelerograms gave similar profiles of a_{max}/a_{base} characterised by significant amplification in the topmost third of the dam, slight de-amplification in the central third and about unit ratio in the lower third. The maximum values of the amplification ratio were obtained at the crest of the dam and

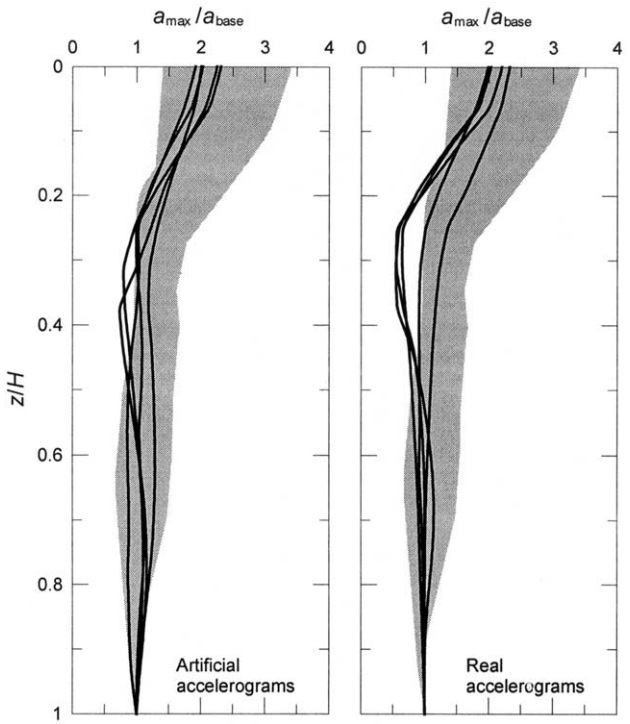

Fig. 22. Comparison with literature results.

are in the range 2.0–2.3. The shaded area in the figure represents the envelope obtained from 13 dam response analyses published in the literature. More specifically, these include the results of linear inelastic shear beam analyses of an ideal earth dam [28] and the results of 2D FE linear equivalent analyses; the latter refer to ideal earth dams [27,32], the Sürgü earth dam [12] and the Santa Juana concrete-face gravel dam [8] and to ideal and real rockfill dams [6,7]. The height of the examined dams ranged between 40 and 150 m. Results of this study are consistent with those given in the literature, and plot close the lower bound that refers to low height earth dams.

Table 10 reports the amplification ratio obtained from crest and base accelerations measured at some instrumented dam sites; these are in the range of 1.5–10. The highest values of the amplification ratio generally refer to stiff rockfill dams subjected to weak motions that mostly deform in the range of pseudo-linear soil behaviour. The values of the amplification ratio determined in this study are close to those measured for the Sannokai dam and Long Valley dam, characterised by embankment material and height similar to those of the Marana Capacciotti earth dam.

As shown in Figs. 18 and 19, high values of the maximum acceleration were obtained close to the upstream and downstream slopes, the maximum values being attained in the lower portions of the dam; this is consistent with other dynamic FE analyses [6] and may be attributed to low values of the confinement stress. Accordingly, 2D response analysis showed values of the shear strain as high as about 0.6% down to a depth of 8–10 m from the upstream and downstream slopes, while values of $\gamma_{av} \leq 0.2–0.3\%$, compatible with or only slightly greater than the volumetric threshold, were obtained for most of the dam body. Levels of shear strain higher than the volumetric threshold might imply pore pressure build-up during the earthquake. However, measurements of Δu carried out in RC tests indicate that for values of $\gamma \approx 0.6\%$ the excess pore water pressure is $<10–13\%$ of the mean effective stress and is likely to induce negligible effects on the shear strength. Moreover, it is worth noting that some constructive features are likely to prevent any seismic-induced pore pressure build-up within the dam body; specifically, in the upstream portion excess pore water pressure can only develop underneath the rockfill cover, about 3–4 m thick, while the downstream portion of the dam is kept drained by the central sub-vertical drain and by the downstream drain at the toe.

The larger displacements were obtained from the 1D response analysis, assuming the bedrock at a depth of 25 m and using both artificial and real accelerograms; the bedrock depth corresponding to the largest displacements could not be anticipated due to the progressive decrease in frequency induced by non-linear soil behaviour. The maximum vertical displacements were about 8 and 20 cm for the downstream slope and about 5 and 13 cm for the upstream slope; using real accelerograms yields maximum displacements that are about 2.5 times greater than those obtained adopting artificial input motions. This could be ascribed to the stationary frequency content of the artificial accelerograms; hence, caution should be devoted when analysing non-linear systems using such artificial input motions. Displacement evaluation from 1D response analysis is conservative in that yields the largest seismic-induced displacements. This happens because in the 2D analysis the average acceleration history, obtained from equilibrium of forces acting on the elements through the potential sliding surface, results from inertial forces that may be acting in opposite directions at different points within the potential failure mass.

It is well known that the displacement-based analyses do not provide a satisfactory representation of the deformation pattern of an earth dam. However the computed earthquake-induced displacement is a useful index of the potential level of deformation, and permit to compare alternative scenarios of analysis. This is particularly convenient when significant uncertainties are involved in the choice of the input ground

Table 10
Peak accelerations monitored at the base and the crest of real earth and rockfill dams

Dam	Material	Height (m)	Event	a_b/g	a_{crest}/a_b	Reference
El Infiernillo	Rockfill	148	1966	0.02	3.8	Gazetas [28]
			1966	0.02	3.0	
La Villita	Clay core and rockfill shells	60	October 11, 1975	0.07	4.8	Elgamal et al. [10]
			November 15, 1975	0.04	5.0	
			October 25, 1981	0.09	4.9	
			September 19, 1985	0.12	6.6	
			September 21, 1985	0.04	5.1	
Sannokai	Clay core and earth fill	37	May 7, 1964	0.06	3.3	Gazetas [33]
				0.03	2.7	
Kisenyama	Clay core and rockfill shells	95	September 1969	0.01	10	Gazetas and Dakoulas [7]
Santa Felicia	Clay core and sandy gravel shells	83	February 1971	0.22	0.9	Prevost et al. [34]
Long Valley	Silty sand and gravel	38	May 1980	0.17	3.06	Seed [35]
				0.18	2.61	Griffiths and Prevost [36]
Leroy Anderson	Earth and rockfill	72	April 24, 1984	0.42	1.50	Gazetas [28]

motion and bedrock depth, assumed that an accurate geotechnical characterisation is available. Ground response analyses using total-stress linear-equivalent 1D or 2D methods, coupled with block sliding analyses also permit to identify those situations that eventually need to be faced with non-linear effective stress methods of dynamic analyses. For the case at hand, the analyses performed allowed the most critical seismic scenarios to be identified among those considered. The maximum vertical displacement induced by the earthquake loading resulted lower than about 10% of the service freeboard, thus indicating a satisfactory index of seismic performance of the earth dam.

References

[1] Lin JS, Whitman RV. Decoupling approximation to the evaluation of earthquake-induced plastic slip in earth dams. Earthq Engng Struct Dyn 1983;11:667–78.

[2] Gazetas G, Uddin N. Permanent deformation on preexisting sliding surfaces in dams. J Geotech Engng, ASCE 1994;120(11):2041–61.

[3] Rathje EM, Bray JD. An examination of simplified earthquake-induced displacement procedures for earth structures. Can Geotech J 1999;36:72–87.

[4] Rathje EM, Bray JD. Nonlinear coupled seismic sliding analysis of earth structures. J Geotech Geoenviron Engng, ASCE 2000;126(11): 1002–14.

[5] Makdisi FI, Seed HB. Simplified procedure for estimating dam and embankment earthquake-induced deformations. J Geotech Engng, ASCE 1978;104(7):849–67.

[6] Seed HB, Seed RB, Lai SS, Khamenehpour B. Seismic design of concrete faced rockfill dams. Concrete face rockfill dams—design, construction and performance, ASCE; 1985. p. 459–478.

[7] Gazetas G, Dakoulas P. Seismic analysis and design of rockfill dams: state-of-the-art. Soil Dyn Earthq Engng 1992;11:27–61.

[8] Troncoso JH, Krause AJ, Corser PG. Seismic design of lined face earth dams. Proceedings of Second International Conference on Earthquake Geotechnical Engineering, Lisbon: Balkema; 1999. p. 703–9.

[9] Chopra AK, Zhang L. Earthquake-induced base sliding of concrete gravity dams. J Struct Engng, ASCE 1991;117(12):3698–719.

[10] Elgamal AWM, Scott RF, Succarieh MF, Liping Y. La Villita dam response during five earthquakes including permanent deformations. J Geotech Engng, ASCE 1990;116(10):1443–62.

[11] Bardet JP, Davis CA. Performance of San Fernando dams during 1994 Northridge earthquake. J Geotech Engng, ASCE 1996;120(7): 554–64.

[12] Özkan MY, Erdik M, Tunçer MA, Yilmaz Ç. An evaluation of Sürgü dam response during 5 May 1986 earthquake. Soil Dyn Earthq Engng 1996;15:1–10.

[13] Calabresi G, Rampello S, Sciotti A, Amorosi A. Diga sulla Marana Capacciotti: Verifica delle condizioni di stabilità e analisi del comportamento in condizioni sismiche. Res. Rep. Dip. di Ingegneria Strutturale e Geotecnica, Università di Roma La Sapienza; 2000

[14] Viggiani G. Small strain stiffness of fine grained soils. PhD Thesis. City University, London; 1992

[15] Rampello S, Viggiani G, Silvestri F. The dependence of small strain stiffness on stress state and history for fine grained soils: the example of Vallericca clay. Proceedings of the International Symposium on 'Pre-failure Deformation Characteristics of Geomaterials', vol. 1. Sapporo: Balkema; 1994.

[16] Rampello S, Viggiani GMB. Pre-failure deformation characteristics of geomaterials. Discussion leader report on session 1a: laboratory tests. Proceedings of the Second International Symposium on 'Pre-failure Deformation Characteristics of Geomaterials', vol. 2. Torino: Balkema; 2001. p. 1279–89.

[17] Silva WJ, Lee K. WES RASCAL code for synthesizing earthquake ground motions. State of the art for assessing earthquake hazards in the United States. Miscellaneous paper S-73-1, Report 24, Vicksburg: US Army Corps of Engineers, Waterways Experiment Station; 1987. 120 pp..

[18] Green RK. Selection of ground motions for the seismic evaluation of embankments. In: Seed RB, Boulanger RW, editors. Proceedings of the ASCE Specialty Conference on Stability and Performance of Slopes and Embankments—II. Geotechnical Special Pub. No. 31, vol. I.; 1992. p. 593–607.

[19] Eurocode No. 8. Design provisions for earthquake resistance of structures—part1-1: general rules—seismic actions and general requirements for structures; 1994

[20] Cacciola P, Colajanni P, Muscolino G. Combination of modal responses consistent with seismic input representation. Accepted for publication in the J Struct Engng, ASCE

[21] Shinozuka M. Simulation of multivariate and multidimensional random processes. J Acoust Soc 1970;49.

[22] CNR-GNDT. L'attività del GNDT nel triennio 1993–1995, a cura di. Corsanego A, Faccioli E, Gavarini C, Scandone P, Slejko D, Stucchi M; 1996

[23] Finn WDL. State-of-the-art of geotechnical earthquake engineering practice. Soil Dyn Earthq Engng 2000;20:1–15.

[24] Decanini L, Mollaioli F. Formulation of elastic earthquake input energy spectra. Earthq Engng Struct Dyn 1998;27:1503–22.

[25] Decanini L, Gavarini C, Mollaioli F. Some remarks on the Umbria-Marche earthquakes of 1997. Eur Earthq Engng 2000;3:18–48.

[26] Idriss IM, Sun JI. A computer program for conducting equivalent linear seismic response analyses of horizontally layered soil deposits. Davis: Center for Geotechnical Modeling, Department of Civil and Environmental Engineering, University of California; 1992.

[27] Prato CA, Delmastro E. 1-D Seismic analysis of embankment dams. J Geotech Engng, ASCE 1987;113(8):904–9.

[28] Gazetas G. Seismic response of earth dams: some recent developments. Soil Dyn Earthq Engng 1987;6(1):2–47.

[29] Hudson M, Idriss IM, Beikae M. QUAD4M. A computer program to evaluate the seismic response of soil structures using finite element procedures and incorporating a compliant base. Davis: Center for Geotechnical Modeling, Department of Civil and Environmental Engineering, University of California; 1994.

[30] Newmark NM. Effect of earthquakes on dams and embankments. Geotechnique 1965;15(2):139–60.

[31] Hynes-Griffin ME, Franklin AG. Rationalizing the seismic coefficient method. Miscellaneous paper GL-84-13, Vicksbourg: US Army Corps of Engineers, Waterways Experiment Station; 1984. 21 pp.

[32] Makdisi FI, Kagawa T, Seed HB. Seismic response of earth dams in triangular canyons. J Geotech Engng, ASCE 1982;108(10):1328–37.

[33] Gazetas G. Shear vibration of vertically inhomogeneous earth dams. Int J Numer Anal Meth Geomech 1982;6:219–41.

[34] Prevost JH, Abdel-Ghaffar AM, Elgamal AWM. Nonlinear hysteretic dynamic response of soil systems. J Engng Mech, ASCE 1985;111(7): 882–97.

[35] Seed HB. Lessons from the performance of earth dams during earthquakes. Design of dams to resist earthquake, London: ICE; 1980. p. 251–8.

[36] Griffiths DV, Prevost JH. Two- and three-dimensional dynamic finite element analyses of the Long Valley dam. Geotechnique 1988;38(3): 367–88.